Journal of Chromatography B, 879 (2011) 3310–3316

Contents lists available at ScienceDirect

Journal of Chromatography B

journal homepage: www.elsevier.com/locate/chromb

Computational investigation of the substrate recognition mechanism of protein D-aspartyl (L-isoaspartyl) *O*-methyltransferase by docking and molecular dynamics simulation studies and application to interpret size exclusion chromatography data☆

Ikuhiko Noji[a], Akifumi Oda[a,b], Kana Kobayashi[a], Ohgi Takahashi[a,*]

[a] *Faculty of Pharmaceutical Sciences, Tohoku Pharmaceutical University, 4-4-1 Komatsushima, Aoba-ku, Sendai, Miyagi 981-8558, Japan*
[b] *Institute for Protein Research, Osaka University, 3-2 Yamadaoka, Suita, Osaka 565-0871, Japan*

ARTICLE INFO

Article history:
Received 29 November 2010
Accepted 14 June 2011
Available online 21 June 2011

Keywords:
Protein D-aspartyl (L-isoaspartyl) *O*-methyltransferase
Molecular dynamics
Docking
β-Aspartic acid
D-Amino acid

ABSTRACT

Unusual amino acid residues such as L-β-aspartyl (Asp), D-α-Asp, and D-β-Asp have been detected in proteins and peptides such as α-crystallin in the lens and β-amyloid in the brain. These residues increase with age, and hence they are associated with age-related diseases. The enzyme protein D-aspartyl (L-isoaspartyl) *O*-methyltransferase (PIMT) can revert these residues back to the normal L-α-Asp residue. PIMT catalyzes transmethylation of *S*-adenosylmethionine to L-β-Asp and D-α-Asp residues in proteins and peptides. In this work, the substrate recognition mechanism of PIMT was investigated using docking and molecular dynamics simulation studies. It was shown that the hydrogen bonds of Ser60 and Val214 to the carboxyl group of Asp are important components during substrate recognition by PIMT. In addition, specific hydrogen bonds were observed between the main chains of the substrates and those of Ala61 and Ile212 of PIMT when PIMT recognized L-β-Asp. Hydrophobic interactions between the $(n-1)$ residue of the substrates and Ile212 and Val214 of PIMT may also have an important effect on substrate binding. Volume changes upon substrate binding were also evaluated in the context of possible application to interpretation of size exclusion chromatography data.

1. Introduction

Scientists used to believe that D-amino acids in vital proteins were removed in the evolutionary process and that living organisms currently contain only L-amino acids. However, thanks to analytical technologies developed in recent years, D-amino acids have been widely detected in vital proteins and peptides. In particular, D-aspartyl (D-Asp) and D-serine residues have been detected [1,2]. L-α-Asp residues in proteins and peptides are known to tend to isomerize and/or racemize under physiological conditions [3]. It has been considered that nucleophilic attack of the nitrogen of the following residue to the carboxyl carbon of the L-α-Asp and subsequent dehydration results in an L-succinimide intermediate. The addition of water to this L-succinimide intermediate results in the formation of either L-α-Asp or L-β-Asp. The L-succinimide intermediate can also undergo racemization to yield D-succinimide. From D-succinimide, either D-α-Asp or D-β-Asp can be formed. The formation of succinimide is affected by the nature of the following residue. This reaction easily occurs when the following residue is not sterically bulky, such as Gly, Ala, or Ser [2]. In addition, L-α-Asp residues that are exposed to solvents or located in a more structurally flexible region are more prone to isomerization [2]. Thus, the fact that most of the D-amino acids detected so far are D-Asp is because of the tendency of Asp residues to form succinimide intermediates. The formation of L-β-Asp, D-α-Asp, and D-β-Asp in proteins or peptides causes conformational changes, which may further causes abnormal aggregation, loss of activity, and alteration of sensitivity to proteolysis. Moreover, it has been reported that certain proteins are activated by isomerization [2]. These reactions are related to aging. Representative proteins from which D-Asp residues have been frequently detected include α-crystalline from the lenses of cataract patients and β-amyloid from the brains of Alzheimer's disease patients [1,2,4–6]. In α-crystallin, D-β-Asp residues accumulate with age.

The enzyme protein D-aspartyl (L-isoaspartyl) methyltransferase (PIMT) is present in various prokaryotic and eukaryotic

☆ This paper is part of the special issue "Analysis and Biological Relevance of D-Amino Acids and Related Compounds", Kenji Hamase (Guest Editor).

* Corresponding author at: Faculty of Pharmaceutical Sciences, Tohoku Pharmaceutical University, 4-4-1 Komatsushima, Aoba-ku, Sendai, Miyagi 981-8558, Japan. Tel.: +81 22 727 0208; fax: +81 22 275 2013.
E-mail address: ohgi@tohoku-pharm.ac.jp (O. Takahashi).

1570-0232/$ – see front matter © 2011 Elsevier B.V. All rights reserved.
doi:10.1016/j.jchromb.2011.06.021

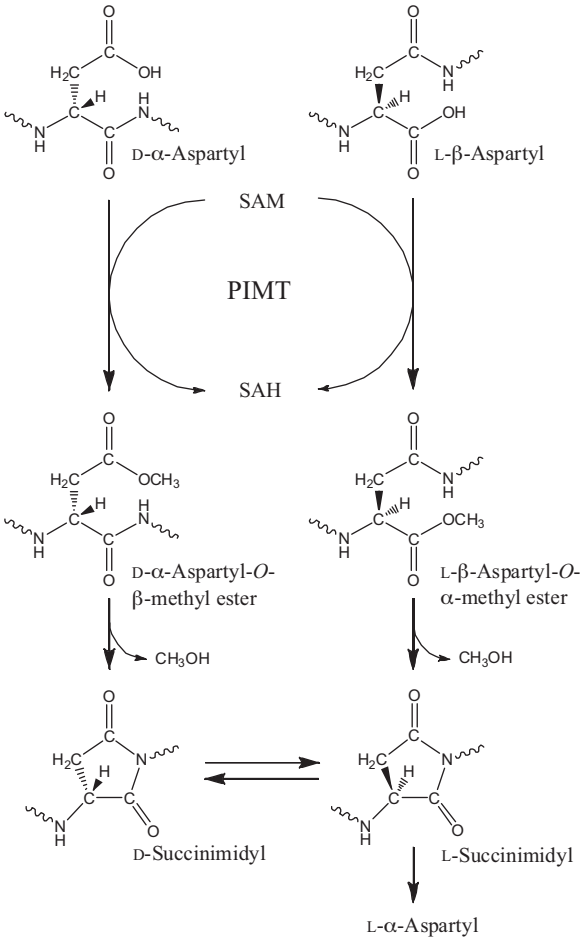

Fig. 1. Reactions of L-β-Asp and D-α-Asp residues initiated by PIMT. PIMT can transfer the methyl group of SAM to the carboxyl group of the side chain. Methanol eliminations from the methylated residues rapidly occur and succinimide intermediates are formed.

organisms. It can initiate the conversion of L-β-Asp or D-α-Asp to L-α-Asp (Fig. 1). PIMT can specifically recognize the carboxyl group of L-β-Asp and D-α-Asp in proteins and peptides and transfer the methyl group of the coenzyme *S*-adenosylmethionine (SAM) to the carboxyl group of the side chain, forming a methyl ester [7–10]. Methylated L-β-Asp and D-α-Asp residues are rapidly converted to L- and D-succinimide intermediates, respectively, with methanol elimination, which can then be converted to L-α-Asp [4–6,11,12]. Although PIMT was originally regarded as a methanol-forming enzyme, it was correctly identified as a protein carboxyl methyltransferase a few years later [5].

The substrate specificity of PIMT varies considerably between species [2,5,13]. For example, mammalian PIMT can recognize both L-β-Asp and D-α-Asp, but PIMT of the hyperthermophilic archaeon *Thermotoga maritima* cannot recognize D-α-Asp. In addition, methylation of D-Asp peptides has not been detected in *Escherichia coli*, worms, or higher plants [14–17]. The substrate affinities for PIMT are different between L-β-Asp and D-α-Asp; the measured Michaelis constant (K_m) of the D-α-Asp peptide is 2–3 orders of magnitude higher than the K_m of the corresponding L-β-Asp peptide [5,14]. PIMT activity has been observed in all mammalian tissues and is particularly high in the brain and testis of rodents. PIMT is produced particularly in the brain, lymph nodes, and pancreas. Because a high level of PIMT has been detected in β-cells, PIMT may be related to type 1 diabetes [18].

PIMT shows a polymorphism at residue 120 [11–13,19]. 120Val PIMT has a higher substrate affinity than 120Ile PIMT, although 120Ile PIMT has a higher thermal stability and is less sensitive to oxidative stress than 120Val PIMT. However, no differences in substrate affinity by the PIMT polymorphism were observed between methyl-accepting peptides.

In studies on PIMT knockout mice, it has been shown that neurotransmission disruptions and development disorders develop by 4 weeks after birth, and these mice finally die because of fatal seizures within 2–3 months after birth [2,5,12]. In the brains of these knockout mice, the β-Asp content was approximately 7–10-fold higher than healthy mice. On the other hand, it has been reported that the expression level of PIMT in the hippocampi of epilepsy patients is less than 50% of that in healthy people, and proteins, including β-Asp, accumulate to an amount 1.5 times greater than in healthy people [2]. Because PIMT activity is high in the testis of rodents and knockout mice fail to mate, these findings may relate to one another. However, it is difficult to perform quantitative analyses of the fertilization competence of knockout mice since they die because of seizures before they reach sexual maturity.

Although PIMT is important for sustaining life activities and procreation, studies on the substrate recognition of PIMT are limited at the molecular level [11–13]. In addition, few structural biology studies have been reported [13]. Ryttersgaard et al. compared the crystal structure of human PIMT with those of *Pyrococcus furiosus* and *T. maritima* [13]. They also performed a docking study using AA(D-Asp) as a substrate; however, there is no (n + 1) residue in this substrate that can affect substrate binding. Furthermore, structural analyses on the recognition of D-α-Asp by human PIMT have yet to be performed. Therefore, we analyzed the specific substrate recognition of PIMT in this work by docking and molecular dynamics (MD) simulation studies. Furthermore, it is proposed that molecular volume calculations by the computational procedure may be useful for interpretation of size exclusion chromatography (SEC) data.

2. Experimental

2.1. Calculations of PIMT–SAM–VYPDHA tertiary complexes

Since no structural information is available on human PIMT–substrate complexes, these complex structures had first to be estimated. We used the human PIMT crystal structure (PDB ID: 1i1n) including *S*-adenosyl homocysteine (SAH) instead of the coenzyme SAM as the initial structure. We added a methyl group to SAH to form SAM, and minimization was then performed on SAM alone. This minimized SAM was re-embedded in PIMT, and only SAM was reminimized. After adding the missing residues (Met1, Ala2, and Lys227) to the PIMT crystal structure, the entire structure was minimized. The PIMT without SAM had a total of 227 residues and total 3517 atoms. On the other hand, the PIMT complex of hyperthermophilic archaeon *P. furiosus* (PDB ID: 1jg3) includes VYP-L-β-Asp-HA as a substrate. Therefore, the PIMT of this complex was replaced with the human PIMT–SAM complex that was already computationally created. The PIMT–SAM–substrate was then minimized and the substrate was removed. From these procedures, a substrate-binding site in PIMT has been prepared. Four peptide substrates and substrate analogues (ligands) – VYP-L-α-Asp-HA (**1**), VYP-L-β-Asp-HA (**2**), VYP-D-α-Asp-HA (**3**), and VYP-D-β-Asp-HA (**4**) – were then docked to the human PIMT–SAM complex. In the present study, the His residues of these peptide ligands were protonated. Since these ligands have been widely used in previous experiments, comparisons can be made with previous experimental data [11–13,20]. From the docking results, the docking poses of the human PIMT–SAM–ligand complexes were screened by comparing the conformations and orientations of the ligands to the PIMT complex of *P. furiosus*. This screening was focused on whether

the carboxyl group of Asp is located near the methyl group of SAM in the active site of PIMT, and whether the orientations of the peptide ligands are similar to that in *P. furiosus*. Since several kinds of docking poses were obtained for each of the four ligands, further screening of the stable structures was performed using MD simulations. If a docking pose is unstable, the ligand will deviate from the protein in the MD simulation.

Minimizations and MD simulations were performed using AMBER 9 (D.A. Case et al., University of California, San Francisco, 2006). The TIP3P water solvent model with a thickness of 8 Å was used. The SHAKE method [21] was used to reduce the computational complexity. The AMBER ff03 force field [22] was used for PIMT, while the general AMBER force field [23] was used for the ligands. MD simulations were performed for 20 ns with a time step of 2 fs at 300 K. A cutoff of 10 Å was used for nonbonding interactions. The particle-mesh Ewald (PME) method was employed to treat the long-range electrostatic interactions. The system was simulated with a periodic boundary condition. LibDock program [24] implemented in Discovery Studio 2.1 (Accelrys, San Diego, 2008) was used for the docking study. The radius of the ligand-binding site was set to 15 Å after considering the length of the hexapeptide ligands. Docking tolerance was set to 0.3 and 0.5 Å, and the number of hotspots was set to 1000. These values were chosen after considering the results of preliminary calculations. The "conformational method" was set to "BEST." As an evaluation of three dimensional (3D) structures of the PIMT–SAM dual complex and the PIMT–SAM–ligand tertiary complexes, volumes of them were calculated in the context of SEC. The volume calculations were carried out by using Mol_Volume program (A. Balaeff, University of Illinois, Urbana-Champaign, 2001), and the probe radius was set to 1.4 Å. For the calculations, the PIMT–SAM complex structure constructed before peptide docking, and the PIMT–SAM–ligand tertiary complexes obtained by 20 ns MD simulations were used.

2.2. Additional tests for substrate binding of PIMT

To confirm the reliability of the results of docking studies and MD simulations of the four PIMT–SAM–VYPDHA complexes, additional tests were carried out using other peptides which are known as substrates of PIMT. The tests were carried out in the same way as for the VYPDHA peptides, i.e., by docking studies and MD simulations. For these additional tests, VYP-L-β-Asp-GA (**5**), SA-L-β-Asp-LA (**6**), and VV-L-β-Asp-SA (**7**) were used as ligand peptides. Peptides **6** and **7** correspond to a partial sequence of the KASA-L-β-Asp-LAKY and KQVV-L-β-Asp-SAYEVIK peptides, respectively, and include the reaction site (L-β-Asp) of these peptides. Peptides **5**, KASA-L-β-Asp-LAKY, and KQVV-L-β-Asp-SAYEVIK are known to be substrates of PIMT [25]. The all parameters and settings of docking and MD simulations for peptides **5**–**7** were the same as those for the VYPDHA peptides mentioned above. In addition, screening procedures for docking pose selections were also the same as those for the VYPDHA peptides. In the calculations for peptides **5**–**7**, the results of the VYPDHA peptides (peptides **1**–**4**) were never referred to, and the calculations were carried out independently. After the additional calculations, the results for peptides **5**–**7** were compared with the results for the VYPDHA peptides.

3. Results and discussion

Three docking poses were obtained for ligand **1**. One of them remained stable during the MD simulation, whereas, for the remaining two poses, the ligands deviated from PIMT during the MD simulation. Three docking poses were also obtained for ligand **2**. In this case, all of these poses were stable during the MD simulation and converged to approximately the same complex structure;

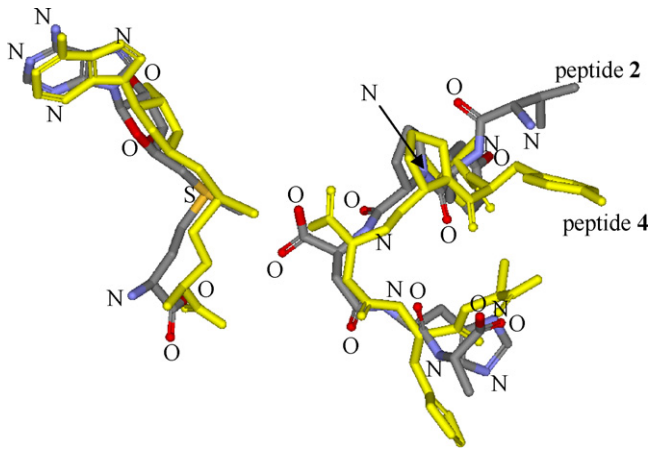

Fig. 2. Superimposition of the complexes including peptide ligands **2** and **4**. Only SAM (left) and the ligands (right) are shown. Structure **2** is colored by element: carbon (gray), nitrogen (blue), oxygen (red), and sulfur (orange). Structure **4** is colored in yellow.

therefore, one of them is shown in the following. Five docking poses were obtained for ligand **3**, but four of them were unstable during the MD simulation and only the one remaining pose was stable. Two docking poses were obtained for ligand **4**, and both of them remained stable during the MD simulation. One of the two complex structures was similar to the structure of PIMT of *P. furiosus* including VYP-L-β-Asp-HA (**2**), and this structure was selected. The root mean square deviations (RMSD) between the initial structures and the MD trajectories were calculated, and it was determined that the four complex structures selected above were stable during MD simulations. In this way, the PIMT–SAM–ligand complex structures including L-α-Asp, L-β-Asp, D-α-Asp, and D-β-Asp in the ligands were chosen.

The conformation and orientation of ligand **2** in the complex structure after MD simulation was very similar to that seen in *P. furiosus*. However, although PIMT cannot recognize D-β-Asp, ligand **4** was located in the approximately the same position as ligand **2** (Fig. 2). Ligands **1** and **3** were bound to PIMT in different ways from ligand **2**, as shown in Fig. 3. This may indicate some diversity of PIMT-binding modes since the active site of PIMT is relatively large.

Fig. 4 shows the hydrogen bonding modes of ligands **1**–**4**. As shown in this figure, all these peptides show a hydrogen bond with Val214. Val214 forms a hydrogen bond with the carboxyl groups of L-α-Asp, L-β-Asp, and D-β-Asp of ligands **1**, **2**, and **4**, respectively. For substrate **3**, Val214 forms a hydrogen bond with the Pro C=O group. In addition, the OH group of Ser60 forms a hydrogen bond with the carboxyl groups of the L-α-Asp, L-β-Asp, and D-α-Asp of ligands **1**, **2**, and **3**, respectively. This hydrogen bond was not observed in ligand **4**. These hydrogen bonds may be important for the recognition of the carboxyl group of the substrates or for fixing their positions. PIMT can recognize both L-β-Asp and D-α-Asp. This could originate from the fact that the hydrogen bonds involving the carboxyl groups of L-β-Asp and D-α-Asp are important for the substrate recoginition of PIMT and the remaining moiety of Asp does not seem to be important. The diversity of the substrate recognitions of PIMT can be attributed to the fact that the crucial hydrogen bonds are to the L-β-Asp or D-α-Asp residues themselves and not to other residues.

Many hydrogen bonds were formed for ligand **2**. It should be noted that hydrogen bonds were formed between the main chain of L-β-Asp and that of Ala61, and between the main chain of His on the C-terminal side of L-β-Asp and that of Ile212 (Fig. 4b). However, these hydrogen bonds were not formed in ligand **4** (Fig. 4d) even though it is bound to PIMT in a position very similar to ligand **2**

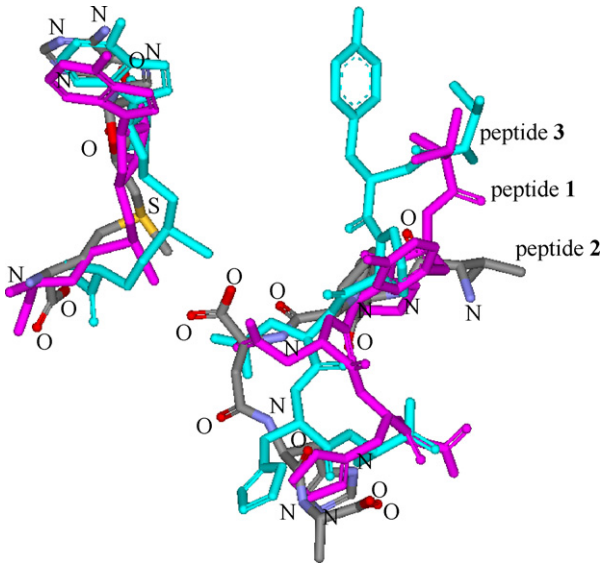

Fig. 3. Superimposition of the complexes including **1**, **2**, and **3**. Only SAM (left) and the ligands (right) are shown. Structure **1** is colored in purple. Structure **2** is colored by element: carbon (gray), nitrogen (blue), oxygen (red), and sulfur (orange). Structure **3** is colored in green.

(Fig. 2). It would appear that the carboxyl group of D-β-Asp of ligand **4** is positioned in a similar manner as L-β-Asp in ligand **2**, resulting in distortion in the main chain, thus disabling the formation of the hydrogen bonds.

Ligands **1** and **3** differed from ligand **2** in their respective hydrogen bonding modes. This is partly because the main chains of ligands **1** and **3** are shorter than those of ligands **2** and **4** by one carbon atom, disabling the formation of the above-mentioned hydrogen bonds (Fig. 4a and c). Therefore, this result suggests that the hydrogen bonds to Ala61 and Ile212 are important factors in the recognition of L-β-Asp by PIMT.

Table 1 shows interatomic distances of the PIMT–SAM–ligand complexes obtained in the MD simulations. The column titled "initial" shows the distances measured before ligand docking. The distance between Pro50 Cγ and Ile212 Cγ in PIMT including ligand **2** were found to become shorter during the MD simulation. This distance was 9.58 Å before the ligand docking and 7.21 Å after MD simulation. In ligand **2**, L-β-Asp and His were located between Pro50 and Ile212, and the distance between Pro50 and Ile212 may have relevance to the specific recognition of L-β-Asp by PIMT. This induced-fit-like reaction was not observed in ligands **1**, **3**, and **4**. Therefore, this reaction, which was only observed with ligand **2**, may be one of the reasons for the high level of affinity of PIMT for L-β-Asp. This indicates that simple docking studies alone can not explain the mechanism of substrate recognition by PIMT. Furthermore, this study demonstrates that MD simulations are essential for refining the complex structures obtained by docking studies and that full-scale MD simulations (of 20 ns for example) are required. Since structural biology experiments on a large number of complexes are too difficult to perform, MD simulations such as those used in this study are important for studying the formation and interaction mechanisms of protein–protein complexes that can result in significant structural changes.

It has been previously reported that hydrophobic groups are favored for the $(n-1)$ residue [12,25]. In the peptides used in this study, the $(n-1)$ residue is Pro. We found that this Pro residue is surrounded by Pro50, Ile212, and Val214, and the proximity of Ile212 and Val214 seems to be because of hydrophobic effects (Fig. 5). Table 1 shows interatomic distances between Pro of the peptide ligands and Ile212 and Val214 of PIMT. The distances between Pro and Val214 for ligands **2** and **4** are shorter than those for ligands **1** and **3**. This indicates that the substrate-binding site of PIMT may have a size and shape that favors β-Asp. These structural changes may be related to the induced fit of PIMT. These results

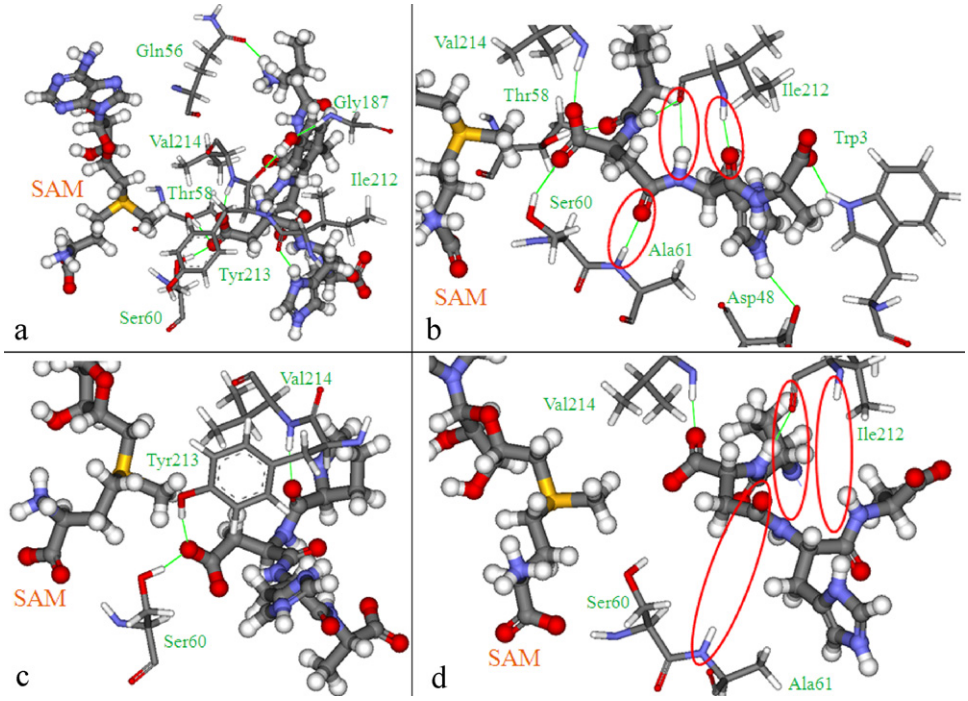

Fig. 4. Hydrogen bonding modes of the four PIMT–SAM–peptide complexes. SAM and peptide ligands are shown as ball and stick models; residues of PIMT are shown as thin stick models. (a) PIMT–SAM–**1** complex. (b) PIMT–SAM–**2** complex. The hydrogen bonds of the main chains of Ala61 and Ile212 to those of L-β-Asp and His, respectively, are indicated by red circles. Hydrogen bonds are shown as green lines. (c) PIMT–SAM–**3** complex. (d) PIMT–SAM–**4** complex. The main chains of Ala61 and Ile212 do not form hydrogen bonds with those of D-β-Asp and His, respectively, as indicated by red circles.

Table 1
Interatomic distances (Å) between residues around the active site of PIMT and between PIMT and ligands in 20-ns MD simulations.

	Initial	VYP-L-α-Asp-HA (**1**)	VYP-L-β-Asp-HA (**2**)	VYP-D-α-Asp-HA (**3**)	VYP-D-β-Asp-HA (**4**)
Distance changes in PIMT					
Pro50 Cγ–Ile212 Cγ	9.58	9.49	7.21	13.95	11.99
Ser60 Cβ–Tyr213 Cβ	8.29	6.96	7.68	9.45	10.17
Thr58 Cβ–Val214 Cβ	6.50	5.67	6.22	7.63	7.66
Pro in ligand–PIMT-binding site distances					
Pro Cβ–Ile212 Cβ	–	10.20	5.23	6.20	4.99
Pro Cβ–Ile212 Cγ1	–	11.31	5.47	7.53	4.46
Pro Cβ–Ile212 Cγ2	–	10.04	6.54	5.09	4.67
Pro Cγ–Ile212 Cγ1	–	11.47	6.43	7.04	5.49
Pro Cγ–Ile212 Cγ2	–	10.32	7.25	4.56	5.96
Pro Cβ–Val214 Cγ1	–	6.27	4.02	6.51	4.43
Pro Cγ–Val214 Cγ1	–	7.31	4.12	6.09	3.67

explain why the hydrophobic interactions of the $(n-1)$ residue of the substrate are important for the substrate recognition of PIMT. PIMT has a structure that prefers L-β-Asp, and substrates including β-Asp can strongly bind to PIMT through hydrophobic interactions. Thus, we considered that the transmethylation reaction by PIMT occurs more easily in L-β-Asp substrates than in D-α-Asp substrates.

The active site of PIMT is formed by Thr58, Ser60, Tyr213, and Val214. This active site became larger by binding to ligands **3** and **4**, as can be seen by the distances between Ser60 Cγ and Tyr213 Cβ and between Thr58 Cβ and Val214 Cβ (Table 1). This may indicate that when substrates including D-Asp are recognized by PIMT, the active site of PIMT must change its size and shape remarkably. However, D-α-Asp can be recognized by PIMT. Therefore, the structural changes that occur in the recognition of D-α-Asp by PIMT may be the result of induced fit.

As described above, when PIMT recognizes substrates, the hydrogen bonds of Ser60 and Val214 to the carboxyl group of Asp are important. In the recognition of L-β-Asp by PIMT, specific hydrogen bonds were observed between the main chain of the substrate and those of Ala61 and Ile212. In addition, hydrophobic interaction between the $(n-1)$ residues of the substrates and the Ile212 and Val214 residues of PIMT may have an important effect on substrate binding. These results are expected to be useful in ascertaining the specific substrate recognition mechanism of PIMT.

In Table 2, the results of volume calculations for the PIMT–SAM dual complex and the PIMT–SAM–peptide tertiary complexes are shown. The changes in volumes caused by complex formation, i.e., diferences between the volumes of the tertiary complexes and the PIMT–SAM dual complex, are also described. For all the four peptide ligands, the volumes increased when the PIMT system formed the tertiary complexes. Although the molecular weights of all the four peptides are the same, volume changes upon complex formation are different between the peptides. For example, the volume change for PIMT–SAM–peptide **3** was larger than twice that for PIMT–SAM–peptide **2**, even though both of the peptides **2** and **3** are substrates of PIMT. These results seem to reflect structural changes induced by formation of the tertiary complexes, and are consistent with the induced-fit-like structural features mentioned above, e.g., the change of the distance between Pro50 Cγ and Ile212 Cγ. As shown in the table, the volume changes can be predicted by using docking studies and MD simulations, even if the molecular weights of complex systems are the same. Thus, the computational docking and MD simulations are expected to be useful for interpretation of experimental data obtained by SEC. Although complex formation can be observed by SEC experiments [26], atomic-level structures of the complexes cannot be obtained. In the interpretation of SEC data, the molecular "size" is generally represented by the molecular weight. However, the actual molecular size (i.e., volume) does not necessarily correspond to the molecular weight, and it may be sometimes possible that detailed interpretation of SEC data cannot be carried out only by using molecular weights. For example, because the molecular weight of PIMT–SAM–peptide **2** is the same as PIMT–SAM–peptide **3**, SEC data about these complexes would be difficult to interpret. As previously explained, docking studies and MD simulations are expected to be useful for such situations. Because the experimental studies to obtain atomic-level structures of protein–protein complexes in liquid phase are difficult and very costly, the collaborations between computational methods and experimental separation techniques, such as SEC, seem to be promising approaches for investigations of protein–protein interactions in liquid phase.

For peptides **5**–**7**, the structures around ligand binding sites of the PIMT–SAM–peptide complexes after 20 ns MD simula-

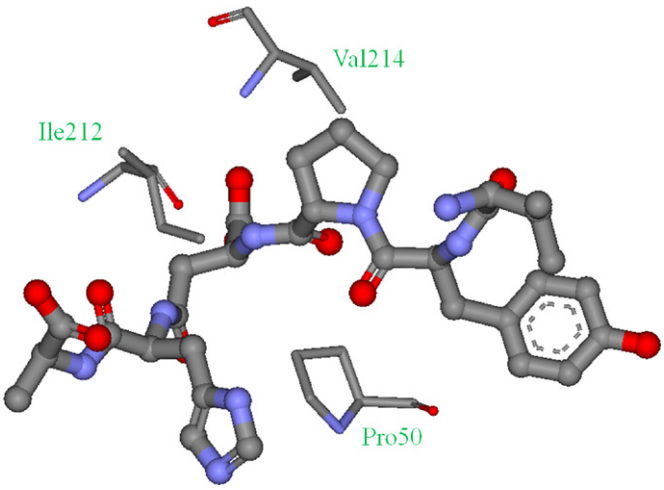

Fig. 5. Interactions between ligand **2** and Pro50, Ile212, and Val214 of PIMT. Because the $(n-1)$ residue of ligand **2**, Pro, is surrounded by Pro50, Ile212, and Val214, hydrophobic effects appear to play important roles in ligand binding.

Table 2
Volumes (Å^3) of PIMT–SAM and PIMT–SAM–peptide complexes.

	Volume	Volume change upon peptide complexation[a]
PIMT–SAM	44,219.0	0 (before complexation)
PIMT–SAM–**1**	45,673.8	1454.8
PIMT–SAM–**2**	45,063.5	844.5
PIMT–SAM–**3**	45,921.4	1702.4
PIMT–SAM–**4**	45,906.2	1687.2

[a] The difference of volumes between the PIMT–SAM dual complex and the PIMT–SAM–peptide tertiary complex.

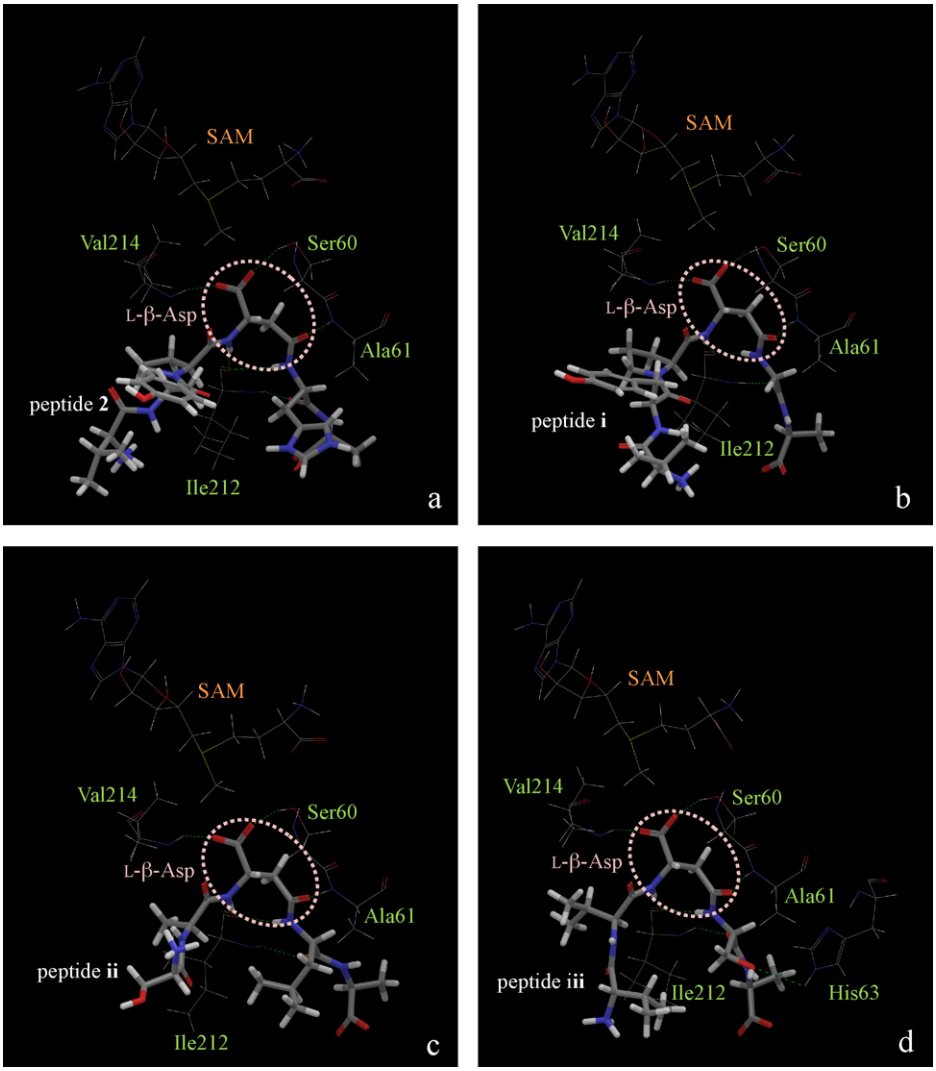

Fig. 6. Binding modes of peptide substrates **2** and **5**–**7**. The peptide ligands are shown as stick models, and PIMT including SAM are illustrated as thin wire models. The hydrogen bonds are represented by green dashed lines. The L-β-Asp residues of the peptide ligands are circled by pink dotted lines. (a) PIMT–SAM–peptide **2** complex. (b) PIMT–SAM–peptide **5** complex. (c) PIMT–SAM–peptide **6** complex. (d) PIMT–SAM–peptide **7** complex. The hydrogen bonding patterns shown in (b)–(d) are similar to that in (a).

tions are illustrated in Fig. 6. For comparison, the structure of PIMT–SAM–peptide **2** complex is also shown. In the figure, the Ser60, Ala61, Ile212, and Val214 residues of PIMT are illustrated in addition to the peptide substrates and SAM. For peptide **7**, the His63 residue is also displayed. As shown in the figure, binding modes of peptides **5**–**7** to the active site of PIMT are similar to that of peptide **2**, although the docking studies and MD simulations for peptides **5**–**7** were carried out independently from peptide **2** without referring to the results for it. That is, the hydrogen bonds between the peptide ligands and the Ser60, Ala61, Ile212, and Val214 residues were observed in the calculated complex structures including peptides **5**–**7**, and the combinations of hydrogen donors and acceptors in these complexes also corresponded to those of the complex including peptide **2**. Furthermore, the $(n-1)$ residues (Pro, Ala, and Val in peptides **5**–**7**, respectively) are located into the hydrophobic environment formed by hydrophobic residues of PIMT, such as Ile212 and Val214, and the results are coincident with that for peptide **2**. These results support the presumptions obtained from the calculations for peptides **1**–**4**, that hydrogen bonds and hydrophobic effects caused by Ser60, Ala61, Ile212, and Val214 play important roles in substrate recognition by PIMT. In addition, these additional tests suggest that the docking calculations and MD simulations are useful to predict 3D structures not only for the complexes including VYPDHA peptides but also for the complexes between PIMT and a wide variety of peptide ligands.

Only the $(n+1)$ residue is different between peptides **2** and **5**; it is His in peptide **2** and Gly in peptide **5**. Although in peptide **2** the ionic interaction between the His $(n+1)$ residue and Asp48 of PIMT (see Fig. 4b) was formed, the Gly $(n+1)$ residue in peptide **5** cannot form such interaction with PIMT. Because the experimentally observed binding affinity between PIMT and peptide **2** was reported to be higher than that of peptide **5** [25], the interaction between PIMT and the $(n+1)$ residue may be related to the binding affinity. In peptide **6**, the $(n+1)$ residue is Leu. In the calculated structure of PIMT–SAM–peptide **6** complex obtained by 20 ns MD simulation, the Leu $(n+1)$ residue of peptide **6** is located in a hydrophobic environment formed by hydrophobic residues of PIMT, such as Ile212. The experimentally observed binding affinity between PIMT and the KASA-L-β-Asp-LAKY peptide was reported to be higher than that of peptide **5**. The higher binding affinity may be explained by the hydrophobic effects around the Leu $(n+1)$

residue of peptide **6**. In peptide **7**, the $(n+1)$ residue is Ser, and a hydrogen bond between the Ser $(n+1)$ residue and His63 of PIMT was observed in the calculated structure of the PIMT–SAM–peptide **7** complex obtained by 20 ns MD simulation. The binding affinity of the KQVV-L-β-Asp-SAYEVIK peptide for PIMT is also higher than that of peptide **5**, and the hydrogen bond of the Ser $(n+1)$ residue might play an important role in the strength of binding. As mentioned above, interactions around side chain atoms of the $(n+1)$ residue appear to be related to the binding affinity for the substrates of PIMT, although the previously performed docking study by Ryttersgaard et al. used the tripeptide including no $(n+1)$ residue [13]. However, the interactions around the $(n+1)$ residue do not seem to be critical to complex formations between PIMT and substrates, because peptide **5**, whose $(n+1)$ residue is Gly, is reported to be recognized by PIMT. The hydrogen bonds by Ser60, Ala61, Ile212 and Val214, and hydrophobic effects around the $(n-1)$ residues seem to be more important in the complex formation than the $(n+1)$ residue because they were also preserved in the calculations for peptides **5**–**7**. The results of additional calculations indicate that the interactions around the $(n+1)$ residue play auxiliary roles in substrate binding of PIMT, and the strength of binding is affected by the $(n+1)$ residue.

In conclusion, the binding mode between PIMT and its substrates was investigated using computational docking and MD simulations. Some hydrogen bonds and hydrophobic effects which play important roles in substrate recognitions were identified, and the interactions were conserved in several peptide substrates. In addition, induced-fit-like structural changes and changes of the molecular volume caused by substrate binding were observed by MD simulations. Because these structural changes cannot be simulated by using only normal computational docking procedures, the results indicate that MD simulations are useful for structural bioinformatics studies of protein–protein (peptide) complexes in liquid phase, such as interpretation of SEC data.

Acknowledgments

We would like to thank the editors and reviewers for their warm support about the submission of the revised manuscript from Sendai, Japan, where we have had the serious disaster (Tohoku earthquake, March 11, 2011) during revision of the manuscript.

References

[1] N. Fujii, T. Saito, Chem. Rec. 4 (2004) 267.
[2] T. Furuchi, H. Homma, Yakugaku Zasshi 127 (2007) 1927.
[3] T. Geiger, S. Clarke, J. Biol. Chem. 262 (1987) 785.
[4] S.C. Griffith, M.R. Sawaya, D.R. Boutz, N. Thaper, J.E. Katz, S. Clarke, T.O. Yeates, J. Mol. Biol. 313 (2001) 1103.
[5] C.M. O'Connor, in: F. Tamanoi, S. Clarke (Eds.), The Enzymes, vol. 24, Academic of Dermatology, San Diego, 2006, p. 385.
[6] J.D. Lowenson, S. Clarke, J. Biol. Chem. 267 (1992) 5985.
[7] C.A. Janson, S. Clarke, J. Biol. Chem. 255 (1980) 11640.
[8] P.N. McFadden, S. Clarke, Proc. Natl. Acad. Sci. U.S.A. 79 (1982) 2460.
[9] E.D. Murray Jr., S. Clarke, J. Biol. Chem. 259 (1984) 10722.
[10] D.W. Aswad, J. Biol. Chem. 259 (1984) 10714.
[11] K. Rutherford, V. Daggett, Protein Eng. Des. Sel. 22 (2009) 713.
[12] C.D. Smith, M. Carson, A.M. Friedman, M.M. Skinner, L. Delucas, L. Chantalat, L. Weise, T. Shirasawa, D. Chattopadhyay, Protein Sci. 11 (2002) 625.
[13] C. Ryttersgaard, S.C. Griffith, M.R. Sawaya, D.C. MacLaren, S. Clarke, T.O. Yeates, J. Biol. Chem. 277 (2002) 10642.
[14] N. Thapar, S.C. Griffith, T.O. Yeates, S. Clarke, J. Biol. Chem. 277 (2002) 1058.
[15] J.C. Fu, L. Ding, S. Clarke, J. Biol. Chem. 266 (1991) 14562.
[16] R.M. Kagan, S. Clarke, Biochemistry 34 (1995) 10794.
[17] N. Thapar, S. Clarke, Protein Expr. Purif. 20 (2002) 237.
[18] A.M. Wagner, P. Cloos, R. Bergholdt, P. Boissy, T.L. Andersen, D.B. Henriksen, C. Christiansen, S. Christgau, F. Pociot, J. Nerup, Diabetologia 50 (2007) 676.
[19] C.G. DeVry, S. Clarke, J. Hum. Genet. 44 (1999) 275.
[20] S.C. Griffith, M.R. Sawaya, D.R. Boutz, N. Thapar, J.E. Katz, S. Clarke, T.O. Yeates, J. Mol. Biol. 313 (2001) 1103.
[21] J.-P. Ryckaert, G. Ciccotti, H.J.C. Berendsen, J. Comput. Phys. 23 (1977) 327.
[22] L. Yang, C. Tan, J. Wang, Y. Duan, P. Cieplak, J. Caldwell, P. Kollman, R. Luo, J. Phys. Chem. B 110 (2006) 13166.
[23] J. Wang, R.M. Wolf, J.W. Caldwell, P.A. Kollman, D.A. Case, J. Comput. Chem. 25 (2004) 1157.
[24] D.J. Diller, K.M. Merz Jr., Proteins Struct. Funct. Genet. 43 (2001) 113.
[25] J.D. Lowenson, S. Clarke, J. Biol. Chem. 266 (1991) 19396.
[26] J.S. Philo, AAPS J. 8 (2006) E564.